

# Properties of odd nuclei and the impact of time-odd mean fields: A systematic Skyrme-Hartree-Fock analysis

K.J. Pototzky<sup>1</sup>, J. Erler<sup>1</sup>, P.-G. Reinhard<sup>1</sup>, and V.O. Nesterenko<sup>2</sup>

<sup>1</sup> Institut für Theoretische Physik II, Universität Erlangen-Nürnberg, Staudstr. 7, D-91058 Erlangen, Germany

<sup>2</sup> Laboratory of Theoretical Physics, Joint Institute for Nuclear Research, Dubna, Moscow region, 141980, Russia

Received: date / Revised version: date

**Abstract.** We present a systematic analysis of the description of odd nuclei by the Skyrme-Hartree-Fock approach augmented with pairing in BCS approximation and blocking of the odd nucleon. Current and spin densities in the Skyrme functional produce time-odd mean fields (TOMF) for odd nuclei. Their effect on basic properties (binding energies, odd-even staggering, separation energies and spectra) is investigated for the three Skyrme parameterizations SkI3, SLy6, and SV-bas. About 1300 spherical and axially-deformed odd nuclei with  $16 \leq Z \leq 92$  are considered. The calculations demonstrate that the TOMF effect is generally small, although not fully negligible. The influence of the Skyrme parameterization and the consistency of the calculations are much more important. With a proper choice of the parameterization, a good description of binding energies and their differences is obtained, comparable to that for even nuclei. The description of low-energy excitation spectra of odd nuclei is of varying quality depending on the nucleus.

**PACS.** 21.60.Jz Nuclear density functional theory – 21.10.Dr Binding energies and nuclear masses – 21.10.Pc Single-particle energies

## 1 Introduction

Nuclear density-functional-theory (DFT) in its most prominent versions, Skyrme-Hartree-Fock (SHF), Gogny, and relativistic mean-field (RMF), are widely used theoretical tools for the description of ground states and dynamics of atomic nuclei, see the reviews [1,2,3]. They have reached a high level of quality in description of nuclear properties throughout the nuclear chart and, what is important, do this in a self-consistent manner. The overwhelming majority of applications deal with even-even nuclei which are far simpler to handle than odd ones. Odd nuclei add crucial pieces of new information, e.g. single-particle spectra, and thus are increasingly studied in recent years. A fully self-consistent calculation for odd nuclei has to account for all the terms following from the initial functional. This means, in particular, that contributions of both time-even and time-odd densities from the initial functional are to be used [1,2,3,4,5]. The time-odd densities (current  $\mathbf{j}$ , spin  $\mathbf{s}$ , and vector kinetic-energy  $\mathbf{T}$ ) and related time-odd mean fields (TOMF) do not contribute to the ground state of non-rotating even-even nuclei but can be essential for the ground states of odd and odd-odd nuclei, as well as in nuclear dynamics including nuclear rotation [5,6,7,8] and electric [9,10,11,12], and magnetic [13,14] giant resonances. Moreover, TOMF embrace the crucial terms to restore the local gauge invariance (Galilean invariance in non-relativistic Skyrme and Gogny models) violated by velocity-dependent time-even densities [4,5].

In odd nuclei, TOMF contribute to the ground state mean fields and, by breaking the time-reversal symmetry in the intrinsic frame, destroy the Kramer's degeneracy of the single-particle states. TOMF might also influence the single-particle spectra and such characteristics as binding energies, odd-even staggering, and separation energies. Note that binding energies and separation energies are important for astrophysical applications [3,15], the odd-even staggering determines the quality of the pairing description [16,17,18,19,20,21,22], the separation energies are crucial for estimation of nuclear stability in drip line [23] and super-heavy regions [24], and the low-energy single-particle spectra are now in focus of exploration of exotic nuclei [23,25].

The role of TOMF in odd nuclei has been already thoroughly inspected for RMF models, see e.g. the recent study [26] and references therein. Most applications of SHF models neglect TOMF. There are a few early publications [18,27] taking care of TOMF, however, involving only light nuclei and a limited number of Skyrme forces (SIII [28] and SLy4 [29]). The large interest on a proper description of odd nuclei motivates a fresh look at the case. Thus very recently, a new SHF study of rare-earth odd nuclei has been published [30], where the TOMF effect on excitation spectra of odd nuclei was discussed in detail. Altogether the previous studies have found rather weak influence of TOMF on properties of odd nuclei. The maximal effect was obtained in light nuclei [18,26]. For bind-

ing energy, the TOMF were shown to give more binding within RMF [26] and effects of both sign within SHF [18]. The TOMF-induced changes in the single-particle spectra were found very small [26,30]. It was claimed that RMF results much less depend on the force parameterization than SHF ones [26].

The previous studies were limited by particular mass regions or specific features of odd nuclei. At the same, it would be very instructive to have a general view of the problem, covering most of the nuclear chart and involving all the basic characteristics which might be affected by TOMF. Just this aim is pursued in the present paper devoted to a systematic exploration of TOMF effects in SHF calculations for proton and neutron odd nuclei. The study covers about 1282 odd nuclei with  $16 \leq Z \leq 92$  (from sulfur to uranium) where experimental energy data are available. Both spherical and axially deform nuclei are involved. Three Skyrme parameterizations SkI3 [31], SLy6 [29], and SV-bas [32] with essentially different effective masses ( $m^*/m=0.58, 0.69, \text{ and } 0.9$ , respectively) are applied. A variety of observables (binding energies, odd-even staggering of energies, separation energies, and low lying single-particle spectra) are analyzed. To separate the effects from time-odd spatial current  $\mathbf{j}$  and spin density  $\mathbf{s}$ , the time-odd terms in the Skyrme functional are sorted into the minimal set for restoring Galilean invariance, and the sets with additional spin and spin-gradient couplings. The results are compared with previous studies in SHF [18,30] and RMF [26].

The paper is outlined as follows. In Sec. 2, the theoretical framework and calculation scheme are outlined. In particular, the Skyrme functional with the time-odd terms and the pairing functional are presented. Results of the calculations are discussed in Sec. 3. The summary is given in Sec. 4. Some details concerning the functional parameters and single-particle wave functions are done in Appendices A and B.

## 2 Model and details of calculations

The starting point is the total energy  $E$  of system [1,3]

$$E = \int d\mathbf{r} \left\{ \mathcal{H}_{\text{kin}}(\tau_q) + \mathcal{H}_{\text{Sk}}(\rho_q, \tau_q, \mathbf{s}_q, \mathbf{j}_q, \mathbf{J}_q, \mathbf{T}_q) \right. \\ \left. + \mathcal{H}_{\text{pair}}(\chi_q) + \mathcal{H}_{\text{C}}(\rho_p) \right\} - E_{\text{cm}}, \quad (1)$$

involving local time-even (nucleon  $\rho_q$ , kinetic-energy  $\tau_q$ , spin-orbit  $\mathbf{J}_q$ ) and time-odd (current  $\mathbf{j}_q$ , spin  $\mathbf{s}_q$ , spin kinetic-energy  $\mathbf{T}_q$ ) densities, as well as the pairing density  $\chi_q$ . The label  $q$  denotes protons and neutrons.

Total densities, like  $\rho = \rho_p + \rho_n$ , have no the index. Further

$$\mathcal{H}_{\text{kin}} = \sum_q \frac{\hbar^2}{2m_q} \tau_q(\mathbf{r}), \quad (2)$$

$$\mathcal{H}_{\text{pair}} = \frac{1}{4} F(\mathbf{r}) \sum_q V_{\text{pair},q} \chi_q^*(\mathbf{r}) \chi_q(\mathbf{r}), \quad (3)$$

$$\mathcal{H}_{\text{C}} = \frac{e^2}{2} \int d\mathbf{r}' \rho_p(\mathbf{r}) \frac{1}{|\mathbf{r} - \mathbf{r}'|} \rho_p(\mathbf{r}') \\ - \frac{3}{4} e^2 \left( \frac{3}{\pi} \right)^{\frac{1}{3}} [\rho_p(\mathbf{r})]^{\frac{4}{3}}, \quad (4)$$

$$E_{\text{cm}} = \frac{\langle \hat{\mathbf{P}}_{\text{cm}}^2 \rangle}{2mA}, \quad (5)$$

are kinetic-energy, pairing, Coulomb, and center-of-mass terms. Note that the center-of-mass energy  $E_{\text{cm}}$  is not included in the mean-field equations but evaluated a posteriori [32]. The pairing interaction may be density dependent (surface pairing with  $F = 1 - \rho/\rho_0$  and  $\rho_0 = 0.20113 \text{ fm}^{-3}$ ) or not (volume pairing with  $F = 1$ ) [19].

The key part of (1) is the Skyrme functional  $\mathcal{H}_{\text{Sk}}$  composed from the terms

$$\mathcal{H}_{\text{Sk}}^{(\text{even})} = \frac{b_0}{2} \rho^2 - \frac{b'_0}{2} \sum_q \rho_q^2 \\ + b_1 \rho \tau - b'_1 \sum_q \rho_q \tau_q \\ - \frac{b_2}{2} \rho \Delta \rho + \frac{b'_2}{2} \sum_q \rho_q \Delta \rho_q \\ + \frac{b_3}{3} \rho^{\alpha+2} - \frac{b'_3}{3} \rho^\alpha \sum_q \rho_q^2 \\ - b_4 \rho \nabla \mathbf{J} - b'_4 \sum_q \rho_q \nabla \mathbf{J}_q \\ - \tilde{b}_1 \mathbf{J}^2 - \tilde{b}'_1 \sum_q \mathbf{J}_q^2, \quad (6)$$

$$\mathcal{H}_{\text{Sk}}^{(\text{Gal})} = -b_1 \mathbf{j}^2 + b'_1 \sum_q \mathbf{j}_q^2 \\ - b_4 (\nabla \times \mathbf{j}) \cdot \mathbf{s} - b'_4 \sum_q (\nabla \times \mathbf{j}_q) \cdot \mathbf{s}_q \\ + \tilde{b}_1 \mathbf{s} \cdot \mathbf{T} + \tilde{b}'_1 \sum_q \mathbf{s}_q \cdot \mathbf{T}_q, \quad (7)$$

$$\mathcal{H}_{\text{Sk}}^{(\text{s}^2)} = \frac{\tilde{b}_0}{2} \mathbf{s}^2 - \frac{\tilde{b}'_0}{2} \sum_q \mathbf{s}_q^2 \\ + \frac{\tilde{b}_3}{3} \rho^\alpha \mathbf{s}^2 - \frac{\tilde{b}'_3}{3} \rho^\alpha \sum_q \mathbf{s}_q^2, \quad (8)$$

$$\mathcal{H}_{\text{Sk}}^{(\text{s}\Delta\mathbf{s})} = -\frac{\tilde{b}_2}{2} \mathbf{s} \cdot \Delta \mathbf{s} + \frac{\tilde{b}'_2}{2} \sum_q \mathbf{s}_q \cdot \Delta \mathbf{s}_q \quad (9)$$

where  $b_i$ ,  $b'_i$ ,  $\tilde{b}_i$ ,  $\tilde{b}'_i$  are the force parameters. Their connection with the standard Skyrme parameters  $t_i$  and  $x_i$  is specified in the Appendix A. The dominant Skyrme contribution  $\mathcal{H}_{\text{Sk}}^{(\text{even})}$  involves only time-even densities  $\rho_q$ ,  $\tau_q$ , and  $\mathbf{J}_q$ . It embraces all standard terms relevant for the ground state properties and electric excitations of even-even nuclei (for electric modes the current  $\mathbf{j}_q$  can be also important [9,10,12]). The isovector spin-orbit interaction is usually linked to the isoscalar one by  $b'_4 = b_4$  and the tensor spin-orbit terms  $\propto \tilde{b}_1, \tilde{b}'_1$  are often omitted [1,3]. For the sake of simplicity we also omit them and the present study and so use  $\tilde{b}_1 = 0$  and  $\tilde{b}'_1 = 0$  throughout.

The next Skyrme contributions,  $\mathcal{H}_{\text{Sk}}^{(\text{Gal})}$ ,  $\mathcal{H}_{\text{Sk}}^{(\text{s}^2)}$ ,  $\mathcal{H}_{\text{Sk}}^{(\text{s}\Delta\text{s})}$ , add gradually terms with the time-odd densities  $\mathbf{j}_q$ ,  $\mathbf{s}_q$ , and  $\mathbf{T}_q$  and create corresponding TOMF in the mean-field equations. These are the terms of our particular interest. They do not contribute to ground state properties of even-even nuclei but become relevant in odd nuclei and nuclear dynamics (rotation, electric and magnetic giant resonances). In the present study we consider three options for the TOMF impact:

$$\mathcal{H}_{\text{Sk}}^{(\text{even})}, \quad (10)$$

$$\mathcal{H}_{\text{Sk}}^{(\text{min})} = \mathcal{H}_{\text{Sk}}^{(\text{even})} + \mathcal{H}_{\text{Sk}}^{(\text{Gal})}, \quad (11)$$

$$\mathcal{H}_{\text{Sk}}^{(\text{min+s}^2)} = \mathcal{H}_{\text{Sk}}^{(\text{even})} + \mathcal{H}_{\text{Sk}}^{(\text{Gal})} + \mathcal{H}_{\text{Sk}}^{(\text{s}^2)}. \quad (12)$$

The first option deals only with  $\mathcal{H}_{\text{Sk}}^{(\text{even})}$ , i.e. involves only time-even densities. This violates Galilean invariance in nuclear dynamics [4]. Adding the term  $\mathcal{H}_{\text{Sk}}^{(\text{Gal})}$  restores this invariance. This yields  $\mathcal{H}_{\text{Sk}}^{(\text{min})}$ , the minimal set to achieve a consistent dynamical model. Derivation of the functional from a Skyrme force [33,34] also yields the spin terms  $\mathcal{H}_{\text{Sk}}^{(\text{s}^2)}$  and  $\mathcal{H}_{\text{Sk}}^{(\text{s}\Delta\text{s})}$  with the parameters  $\tilde{b}_i$  and  $\tilde{b}'_i$  uniquely related to the  $b_i$ ,  $b'_i$ , see Appendix A. Following our experience, the term  $\mathcal{H}_{\text{Sk}}^{(\text{s}\Delta\text{s})}$  leads to unstable ground states for many medium and heavy nuclei. This is a common problem in most Skyrme parameterizations [35,36]. Thus we include to the option  $\mathcal{H}_{\text{Sk}}^{(\text{min+s}^2)}$  only the simple spin term  $\mathcal{H}_{\text{Sk}}^{(\text{s}^2)}$ . The comparison of results for  $\mathcal{H}_{\text{Sk}}^{(\text{even})}$  with those from  $\mathcal{H}_{\text{Sk}}^{(\text{min})}$  and  $\mathcal{H}_{\text{Sk}}^{(\text{min+s}^2)}$  should provide information on the influence of TOMF. The corresponding total energies are denoted as  $E_{\text{even}}$ ,  $E_{\text{min}}$ , and  $E_{\text{min+s}^2}$ .

The calculations are performed in cylindrical coordinate space grid with the mesh size 1 fm. The axial equilibrium deformations are determined by minimization of the total energy [1]. The calculations are restarted from different initial deformations to separate isomeric and absolute minima of the energy.

To explore the possible variance of the results, the calculations are done for three different Skyrme parameterizations, SkI3 [31], SLy6 [29], and SV-bas [32] with the effective masses  $m^*/m=0.58, 0.69$ , and  $0.9$ , respectively. All the parameterizations provide a reasonable description of stable even-even nuclei and giant resonances, though perform differently with respect to more detailed observables. The force SkI3 is known to reproduce peculiarities of Pb

isotopic chain. SLy6 was developed with special emphasis on neutron rich nuclei and neutron matter. The recent parameterization SV-bas [32] is fitted for a large data set covering long isotopic and isotonic chains and so may be most suited for systematic explorations. Note that SkI3 and SV-bas allow an isovector spin-orbit force (decoupled parameter  $b'_4$ ) while SLy6 fixes that to the isoscalar term by setting  $b'_4 = b_4$ . Both these differences can affect the single-particle shell structure and so the properties of odd nuclei.

The pairing functional (3) uses the volume pairing for SkI3 and SLy6 and surface pairing for SV-bas. The pairing strengths  $V_{\text{pair},q}$  are adjusted following the recipe [32]. The pairing is augmented by the stabilization procedure from [37]. This prevents the breakdown of the pairing near the closed shells which to some extent simulates the similarly smoothing in particle-number projection and so avoids unphysical kinks in properties along collective deformation paths.

The pairing mean-field equations are derived from the given pairing functional and solved in the BCS approximation. The pairing density in (3) is

$$\chi_q(\mathbf{r}) = - \sum_{k \in q} u_k v_k f_k^q \sum_{\sigma=\pm} \sigma \phi_k^{(-\sigma)}(\mathbf{r}) \phi_k^{(\sigma)}(\mathbf{r}) \quad (13)$$

where the sum runs over the single-particle states  $k$ , the state  $\bar{k}$  is time-conjugate to  $k$ ,  $v_k$  and  $u_k$  are Bogoliubov amplitudes,  $\phi_k^{(\sigma)}(\mathbf{r})$  is the spin  $\sigma$ -component of the single-particle wave function in cylindrical coordinates (see appendix B).

The weight in (13)

$$f_k^q = \frac{1}{1 + \exp\{[0.5(\epsilon_k + \epsilon_{\bar{k}}) - \lambda_q - \Delta E_q]/\mu_q\}} \quad (14)$$

is an energy-dependent cut-off factor limiting the pairing space to the vicinity of the Fermi energy. The cut-off is necessary to suppress unphysically large contributions from high-lying states, caused by the zero-range form of the pairing interaction [1]. We use here the recipe [19] with the cut-off parameters amounting in average to the typical values  $\Delta E_q=5$  MeV and  $\mu_q=0.5$  MeV [38]. The value  $\epsilon_k$  is the single-particle energy of state  $k$  and  $\lambda_q$  is the chemical potential.

In odd nuclei, the odd nucleon misses a partner to join the pairing scheme and thus blocks the occupied single-particle state. The blocking results in the one-quasiparticle state [39,40]

$$\hat{\alpha}_{k_1}^+ |\text{BCS}\rangle = \hat{\alpha}_{k_1}^+ \prod_{k>0, k \neq k_1} (u_k + v_k \hat{a}_k^+ \hat{a}_k^+) |0\rangle, \quad (15)$$

where  $\hat{\alpha}_k^+$  and  $\hat{a}_k^+$  are quasiparticle and single-particle creation operators;  $|\text{BCS}\rangle$  and  $|0\rangle$  are BCS and HF vacuum states. The blocking effect is known to be of a crucial importance for odd nuclei [39,40,41].

We compute the blocked states for a variety of single-particle states  $k$  near the Fermi energy. The state with

lowest energy is treated as the ground state while others form the low-energy excitation spectrum of the odd nucleus.

Finally note that time-conjugate states are easily obtained in even-even nuclei as  $\phi_{\bar{k}} = \hat{T}\phi_k$  by using the time-reversal operator  $\hat{T}$ . However, this is not trivial for odd nuclei where the time-reversal invariance is broken. In this case,  $\phi_{\bar{k}}$  is found as the state having maximum overlap with  $\hat{T}\phi_k$ .

### 3 Results and discussion

In this section we present our results for the influence of TOMF on binding energies, odd-even staggering, separation energies, and low-energy spectra of odd nuclei. Three options (10)-(12) with the corresponding total ground state energies,  $E_{\text{even}}$ ,  $E_{\text{min}}$ , and  $E_{\text{min}+s^2}$ , are compared. The same index convention is applied to other observables.

In this study we neglect the coupling with vibrational states of the even-even core [40,41] and nuclear rotation [42,43]. The loss of the corresponding collective correlations can result in underestimation of the total binding energies by 1-2 MeV in soft or deformed nuclei [44,45]. For the variables represented through the differences of the energies (pairing gaps and separation energies) the effect should be much smaller. For single-particle energies the role of the vibrational and rotational coupling can be dramatic [42]. In general it is reduced to much more compressed low-energy spectrum of odd nuclei [40,41]. So we may expect from very beginning for more dilute SHF spectra as compared to the experimental data.

#### 3.1 Binding energies

Results for the binding energies (BE) are given in Figs. 1-4 and Table 1. The experimental data are taken from [46]. To amplify the effects, the energy differences  $\Delta E$  are considered:  $E_{\text{even}} - E_{\text{min}}$  to check the effect of restoration of Galilean invariance,  $E_{\text{even}} - E_{\text{min}+s^2}$  to demonstrate the total TOMF effect when spin terms  $s^2$  are also added, and  $E_{\text{min}+s^2} - E_{\text{exp}}$  to estimate the deviation from the experimental data.

Fig. 1 shows the BE differences for odd Sn isotopes. Following panel a), the restoration of Galilean invariance enhances the binding. The effect is small throughout and practically negligible for SV-bas. This is not surprising as SV-bas with its effective mass  $m^*/m = 0.9$  has smaller coefficients  $b_1$  and  $b'_1$  than SLy6 and SkI3 and hence weaker current contribution  $\sim j^2$ . The additional inclusion of spin terms (panel b) counterweights the extra binding and leads to its modest reduction by 0.1-0.3 MeV. Thus the effects of TOMF on the BE are generally small.

Panel c) of Fig. 1 shows the difference  $E_{\text{min}+s^2} - E_{\text{exp}}$  between theory and experiment in both even and odd Sn isotopes. This difference is much larger than the previous ones and shows remarkable isotopic trends. The typical patterns for SkI3 and SLy6 show a tendency to over-

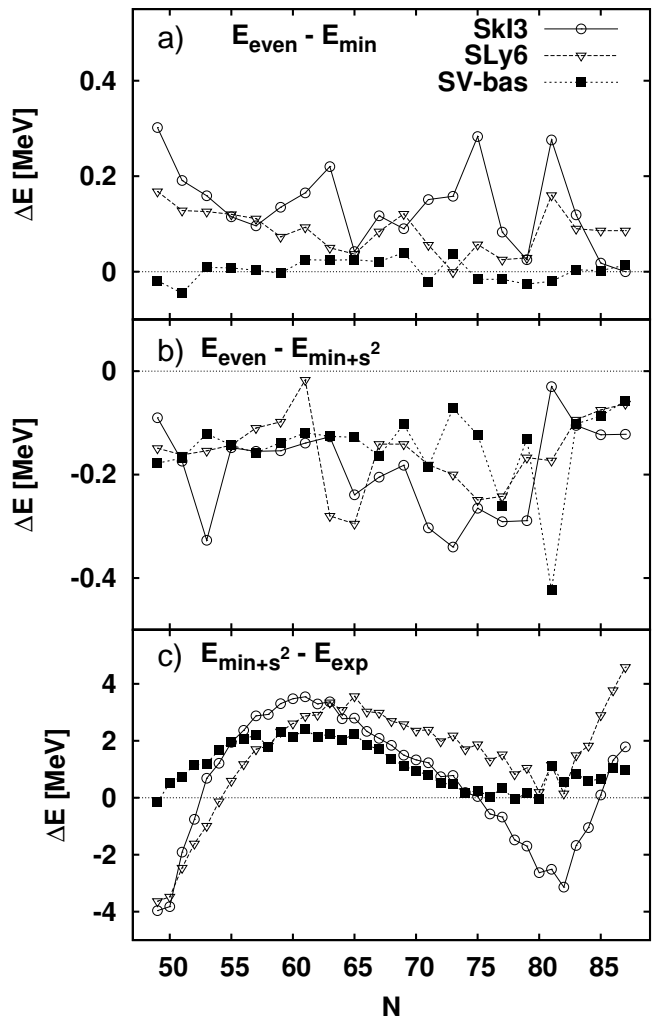


Fig. 1. The energy differences  $E_{\text{even}} - E_{\text{min}}$  (a),  $E_{\text{even}} - E_{\text{min}+s^2}$  (b), and  $E_{\text{min}+s^2} - E_{\text{exp}}$  (c), in odd Sn isotopes for the parameterizations SkI3, SLy6, and SV-bas.

binding at the shell closures  $N=50$  and  $82$  and under-binding at mid shell. The most recent parameterization SV-bas produces the smoothest trends and smallest deviations extending to the limits of known isotopes. This is due including the long isotopic and isotonic chains into the SV-bas fit [32]. Even here there remains a region of under-binding by  $\sim 2$  MeV near  $N=55-65$ . But these nuclei are soft and, as was mentioned above, should additionally acquire just this amount of the collective correlation energy [32,44]. Anyway, we see large deviation from the experiment and strong dependence of the results on the Skyrme parameterization. Both these factors are an order of magnitude stronger than the TOMF effects shown in panels a) and b).

Fig. 2 shows the BE differences for the chain of isotones with the neutron number  $N=82$ . Most of the patterns are much the same as for the isotopic chain in Fig. 1 and so the above remarks can be applied for Fig. 2 as well. The only exception seems to be a different behavior of  $E_{\text{min}+s^2} - E_{\text{exp}}$  for SkI3 and SLy6 in panels c) of Figs.

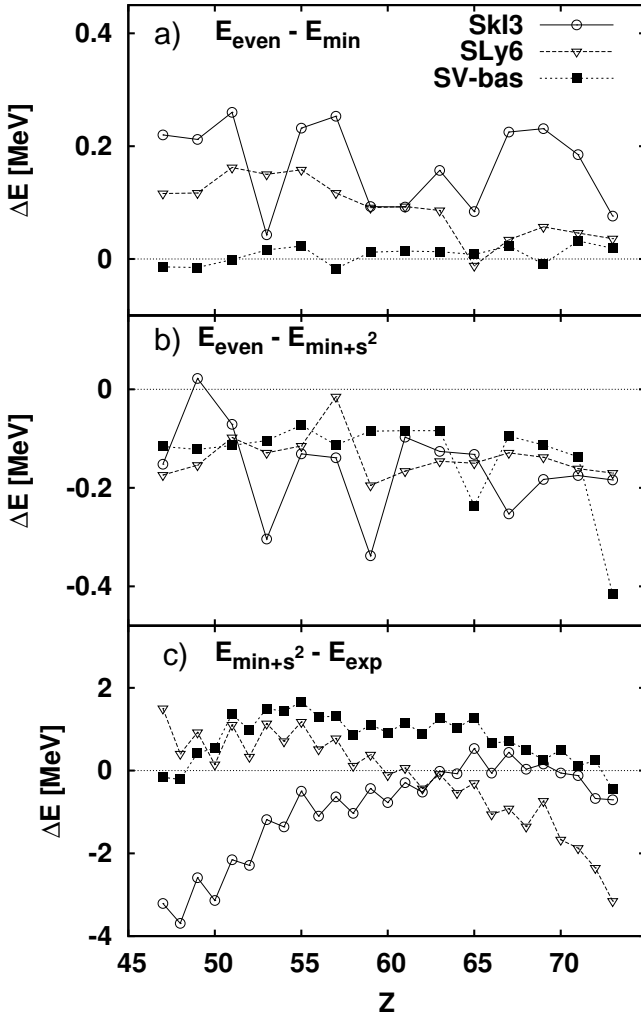


Fig. 2. The same as Fig. 1, but for  $N=82$  isotones.

1 and 2, where we see similar SkI3 and SLy6 trends for isotopes and opposite for isotones. Perhaps, this is related with different fit strategies of these two parameterizations.

In the following we discuss nuclei all over the chart of isotopes, even-even nuclei and proton-odd or neutron-odd ones called henceforth “odd”. Doubly odd nuclei are not considered.

Fig. 3 shows the difference  $E_{\text{even}} - E_{\text{min}+s^2}$  all over the nuclear chart with  $16 \leq Z \leq 92$ . The effect of TOMF is weak everywhere, never exceeding 1 MeV and usually remaining even much smaller. In general the TOMF lead to less binding. The effect is stronger in light nuclei and decreases with the nuclear size, which is in accordance with RMF findings [26]. There is some dependence on the Skyrme parameterization concerning the increase of the TOMF effect for small nuclei, which is more pronounced for SkI3 and less for SV-bas. Note that, in contrast to the previous Skyrme study [18] for light nuclei, neither the RMF [26] nor our calculations find an enhancement of the TOMF effect at  $N=Z$ . Perhaps in our case this is caused by omitting the term  $\mathbf{s} \cdot \Delta \mathbf{s}$  which was taken into account

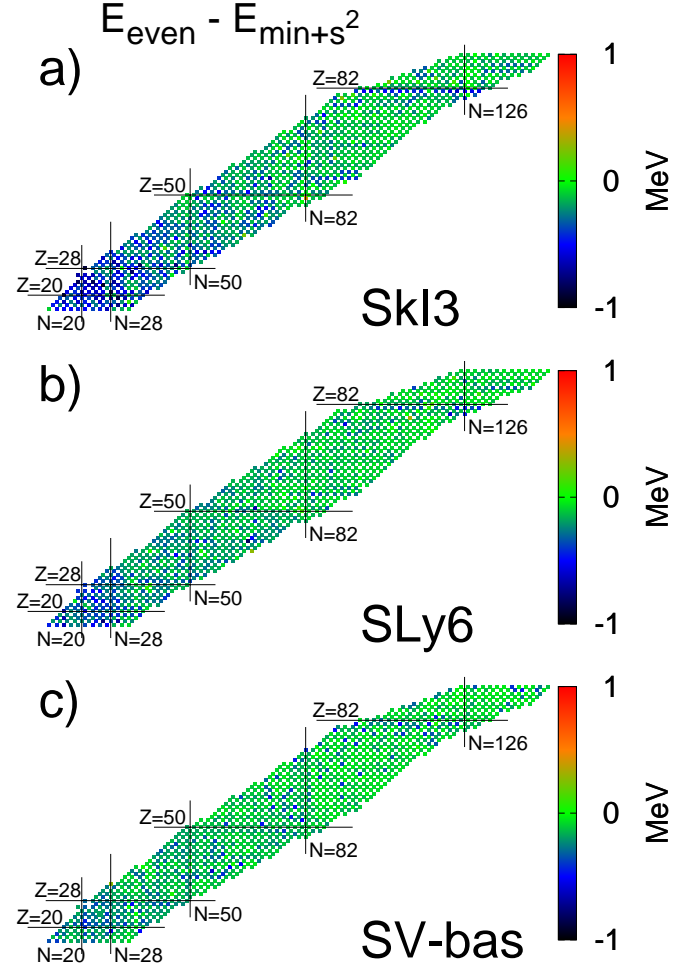
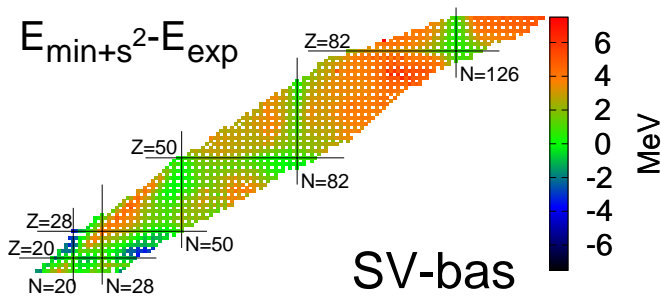


Fig. 3. The binding energy difference  $E_{\text{even}} - E_{\text{min}+s^2}$  for the Skyrme parameterizations SkI3, SLy6 and SV-bas, drawn in the  $N$ - $Z$  plane. All available neutron and proton odd nuclei with the charge  $16 \leq Z \leq 92$  are included.

in [18] and gave there a strong contribution opposite to one from  $s^2$ -terms.

Fig. 4 shows the systematics of the deviation of calculated BE from the experimental data [46] in even and odd nuclei altogether. As all three parameterization show qualitatively the same pattern, we show only the results from SV-bas. As might be expected, the best agreement is found along the isotopic and isotonic chains of semi-magic nuclei. These are the nuclei with least correlation effects [44].

The present calculations omit these effects and generally yield under-binding for deformed nuclei. Subtracting proper correlation energies cures the problem for light and medium nuclei. But there remains a systematic trend to under-binding of deformed heavy and super-heavy elements which is a well known problem of all Skyrme parameterizations [32,47]. The same trends exist for even-even nuclei and for other Skyrme parameterizations. Actually they are features of the present SHF functionals as such. Most important for our purposes is that odd nuclei do not



**Fig. 4.** The difference between SHF and experimental values [46] of the binding energy,  $E_{\min+s^2} - E_{\text{exp}}$ , calculated for the force SkI3 and plotted in the  $N$ - $Z$  plane. All even and odd nuclei with  $16 \leq Z \leq 92$  are included.

**Table 1.** R.m.s. deviations (in MeV) between SHF and experimental data [46] for the binding energies in odd, even, and all (odd + even) nuclei from Figs. 3 and 4.

Parameterization	Option	Nuclei		
		even	odd	all
SkI3	$E_{\text{even}}$	3.51	3.57	3.55
	$E_{\text{min}}$	3.51	3.50	3.50
	$E_{\min+s^2}$	3.51	3.73	3.66
SLy6	$E_{\text{even}}$	4.18	4.01	4.07
	$E_{\text{min}}$	4.18	3.97	4.04
	$E_{\min+s^2}$	4.18	4.14	4.15
SV-bas	$E_{\text{even}}$	2.81	2.72	2.75
	$E_{\text{min}}$	2.81	2.71	2.74
	$E_{\min+s^2}$	2.81	2.84	2.83

change the picture at all. They would merge smoothly into the data from even nuclei without showing any special even-odd effect. Proper tuning of BE in even nuclei thus automatically provides good results for BE in odd nuclei as well.

Additional information on the global quality of BE description is done in Table 1 in terms of r.m.s. deviation from experimental data [46]. The numbers have to be taken with care because they are computed from raw mean-field energies without rotational projection and vibrational correlation energy.

Table 1 shows that restoration of the Galilean invariance (step from  $E_{\text{even}}$  to  $E_{\text{min}}$ ) improves the description only a bit. But adding the  $s^2$ -terms, i.e. stepping to  $E_{\min+s^2}$ , again enhances the deviations. Note that even and odd nuclei are described about with a similar accuracy. SV-bas yields to a better description than SkI3 and SLy6 and, again, the difference between the Skyrme parameterizations is much larger than the TOMF effect.

Finally it is worth to compare our results with the RMF predictions, in particular with the recent study of [26] covering light nuclei with  $18 \leq Z \leq 27$  as well as Ce and Cf isotopes. Like in our case, they predict a weakening of the time-odd effects with increasing nuclear size. At the same time, the RMF calculations in light nuclei demonstrate a profound TOMF effect near the proton drip-line and generally more binding induced by the odd-time fields. These findings are not confirmed by our calculations, in

particular, the Skyrme calculation usually reduce binding when including spin terms. However, we should not overestimate the significance of this discrepancy. In both RMF and Skyrme calculations the TOMF contribution to the binding energies consists of a terms of a different sign and actually the final result is determined by a subtle balance of these terms. Using another parameterization or adding still neglected contributions (like  $\mathbf{s} \cdot \Delta \mathbf{s}$  in the SHF) may change the balance and so magnitude and sign of a weak TOMF effect.

In agreement to the previous SHF study [18], the present calculations demonstrate a strong dependence of the results on the parameterization. This is to a large extent a consequence of using essentially different parameterizations SkI3, SLy6, and SV-bas (which possess much different effective masses and vary also in other features). The RMF results [26], on the other hand, are claimed to be almost independent of the parameterization. But it is ought to mention that the RMF parameterizations in this study are rather similar (all from group A in the classification of [26]). More differences may appear when utilizing other RMF parameterizations which have higher effective masses.

### 3.2 Odd-even staggering (OES)

During last years the odd-even staggering (OES) was a subject of intense investigations within various models involving RMF [17, 26], SHF [16, 18, 19, 20, 21, 22], and Gogny [48, 49] approaches. Being mainly attributed to the pairing, the OES is widely used as a measure of the pairing gap. However, the OES can be also affected by other physical mechanisms (e.g. nuclear deformation or TOMF) which significantly complicates the problem and calls for discrimination of the various influences. For SHF, the TOMF effect on OES was so far explored either indirectly [20] or only for light nuclei [18]. To the best of our knowledge, the present study is the first direct and systematic investigation of the TOMF influence on OES. The experimental values of OES used in the present exploration are obtained by using evaluations [46].

There exist several options for characterizing the OES [39]. We adopt the three-point formulas

$$\Delta_N^{(3)}(Z, N) = \frac{(-1)^N}{2} [E(Z, N-1) - 2E(Z, N) + E(Z, N+1)], \quad (16)$$

$$\Delta_Z^{(3)}(Z, N) = \frac{(-1)^Z}{2} [E(Z-1, N) - 2E(Z, N) + E(Z+1, N)]. \quad (17)$$

It ought to be mentioned that background contributions act differently for centering  $\Delta_{Z,N}^{(3)}$  at even or odd nuclei. When centering at odd- $N$  or odd- $Z$  nucleus, respectively. The three-point formulae have the advantage of canceling the smooth background of mean field contributions. Instead, when being centered on even nuclei, (16)-(17) are likely to contain also significant shell and deformation effects [19, 49].

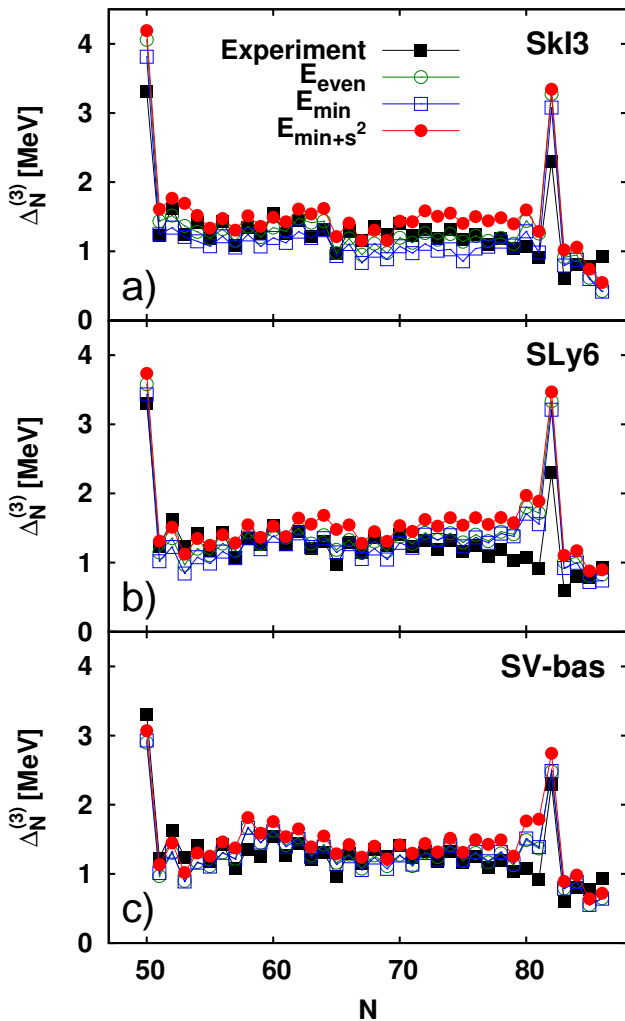


**Fig. 5.** Neutron gaps  $\Delta_N^{(3)}$  in Sn isotopes, calculated for the parameterizations SkI3 (panel a), SLy6 (panel b), and SV-bas (panel c) for the options (10)-(12) as indicated and compared with the experiment [46].

Fig. 5 shows the neutron gaps along the chain of Sn isotopes. All three parameterizations, SkI3, SLy6, and SV-bas, quite accurately describe the OES in sizes and trends. The best agreement is seen in the mid shell regions where pairing dominates in forming the gaps and fit of the pairing strength is accomplished [32]. Larger deviations and a strong dependence on the parameterization are found at and around the shell closures ( $N=50$  and  $82$ ). That is a point where shell effects dominate and the shell structure varies substantially amongst the parameterizations (e.g. due to the much different effective mass). At a more detailed level, one can see that, for SkI3 and SLy6,  $E_{\min}$  slightly underestimates  $\Delta_N^{(3)}$  while  $E_{\min+s^2}$  gives the opposite effect. For SV-bas, both  $E_{\min}$  and  $E_{\min+s^2}$  results are close to experiment. The description is not so perfect for the  $N=82$  isotones shown in Fig. 6 where all three SHF parameterizations show somewhat larger deviations from the experimental data, especially  $E_{\min+s^2}$  for SkI3 and SLy6. But even these deviations are yet quite moderate and one

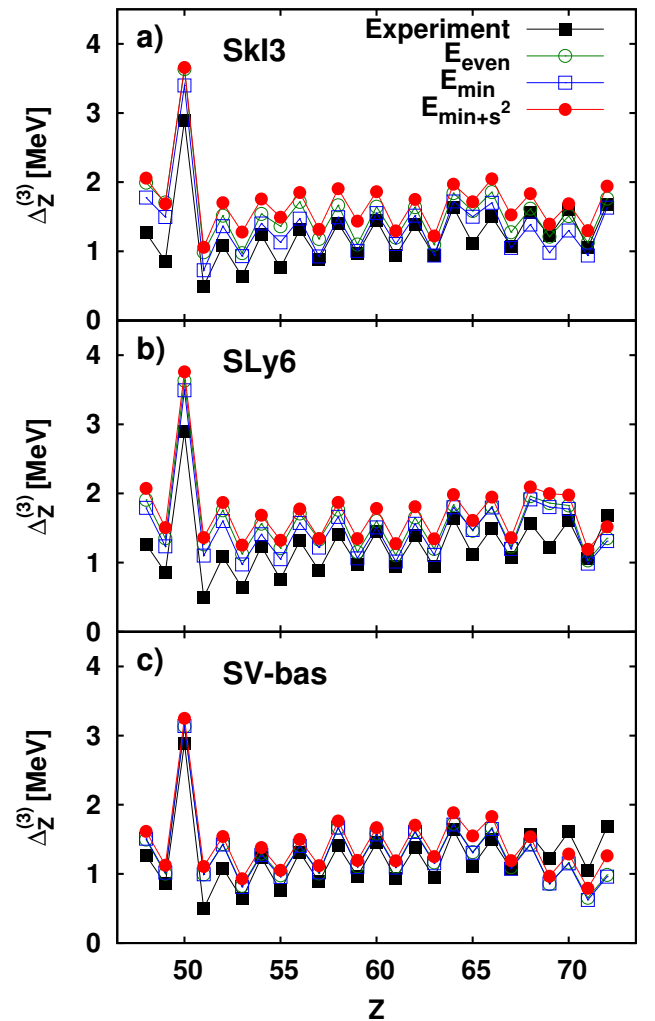


**Fig. 6.** The same as in Fig. 5 for the proton gaps  $\Delta_Z^{(3)}(Z, N)$  in  $N=82$  isotones.

may speak on a generally good description of OES. The trends like a general decrease of  $\Delta_N^{(3)}$  with  $N$  and increase of  $\Delta_Z^{(3)}$  with  $Z$  are reproduced equally well as in the study [21] with the special isospin pairing interaction.

Figs. 7 and 8 show the systematics of the deviations between calculated  $\Delta_N^{(3)}$  (Fig. 7) or  $\Delta_Z^{(3)}$  (Fig. 8) and the experimental data. The majority of nuclei stays in the “green” window having perfect agreement with the data. We see strings of larger deviations along some semi-magic chains and regions of well deformed and transitional nuclei. These nuclei are known to have large collective correlations [44] and are likely to need them for improvement of the gap description. The size of the deviations differs very much amongst the three parameterizations and SV-bas again gives the best results. This is most probably due to the large effective mass ( $m^*/m = 0.9$ ) which seems to produce a more correct level density.

The r.m.s. deviations for OES are summarized in Table 2. Comparison with Table 1 shows that the average deviation for OES is much smaller than for the binding energies, which reflects the fact that OES are less sensi-



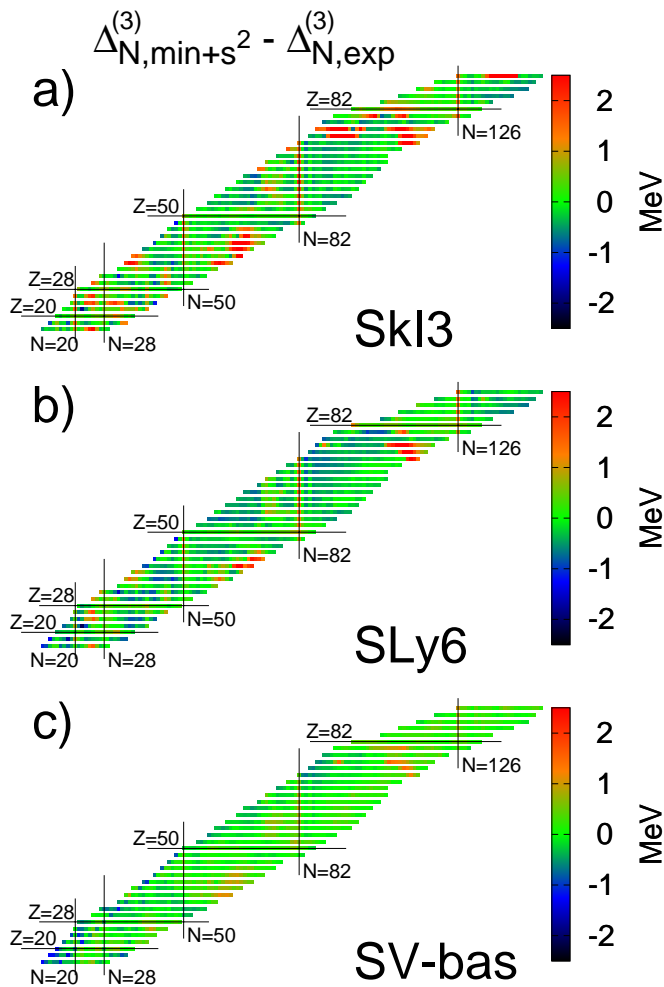


**Fig. 7.** The difference between the theoretical and experimental values [46] of the neutron pairing gaps,  $\Delta_{N,\min+s^2}^{(3)} - \Delta_{N,\exp}^{(3)}$ , for all available nuclei in the window  $16 \leq Z \leq 92$  and for the Skyrme parameterizations SkI3, SLy6, and SV-bas.

tive to nuclear bulk properties and related errors. This is one more example for the fact that energy differences are often more reliably described than a total energy as such [32]. Like for the binding energies in Table 1, the TOMF effect on OES is smaller than variations between the different parameterizations.

### 3.3 Relation between OES and spectral gap

The OES (16)-(17) are closely related to the pairing gaps which appear in the two-quasiparticle excitation spectra of the BCS or HFB calculations [39]. Such spectral gap can be defined as the average [19]

$$\bar{\Delta}_q = \frac{\sum_{k \in q} |u_k v_k \Delta_k|}{\sum_{k \in q} |u_k v_k|}. \quad (18)$$

We use for this purpose  $\Delta_k = \int d\mathbf{r} \phi_k^*(\mathbf{r}) \Delta_q \phi_k(\mathbf{r})$  as the state-dependent gap in even and odd nuclei. The weight

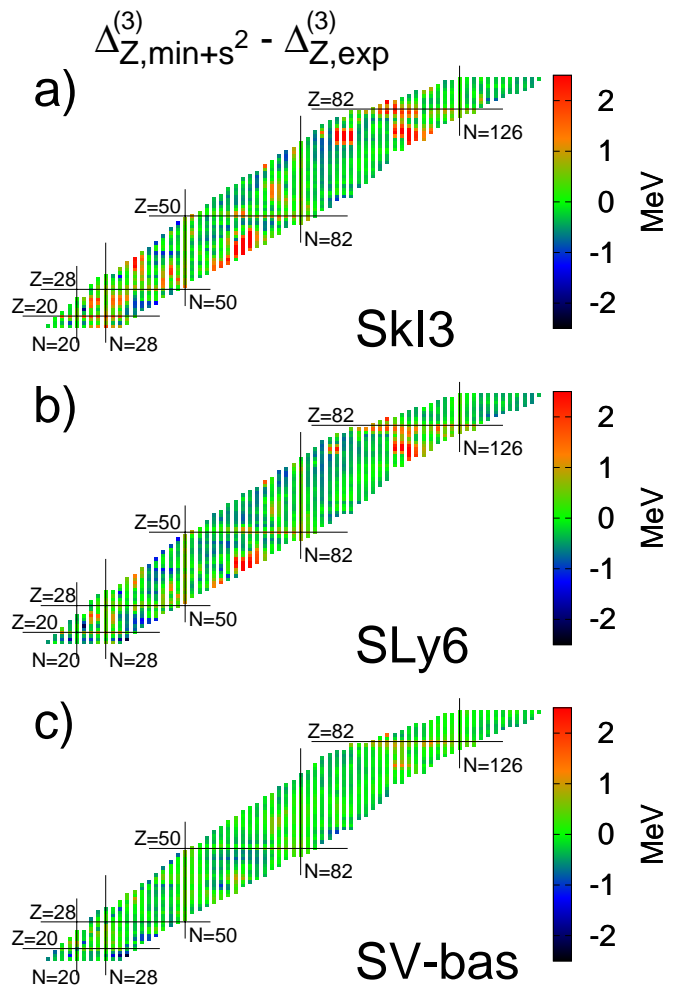


**Fig. 8.** The same as in Fig. 7 for the proton pairing gaps  $\Delta_Z^{(3)}(Z, N)$ .

**Table 2.** R.m.s. deviations (in MeV) between SHF and experimental data [46] for  $\Delta_{N,Z}^{(3)}$  from Fig. 7 and  $\Delta_Z^{(3)}$  from Fig. 8.

$\Delta_N^{(3)}$	SkI3	SLy6	SV-bas
$E_{\text{even}}$	0.98	0.63	0.36
$E_{\text{min}}$	0.97	0.67	0.37
$E_{\text{min}+s^2}$	1.01	0.60	0.36
$\Delta_Z^{(3)}$	SkI3	SLy6	SV-bas
$E_{\text{even}}$	0.79	0.69	0.39
$E_{\text{min}}$	0.82	0.73	0.40
$E_{\text{min}+s^2}$	0.82	0.66	0.35

$u_\alpha v_\alpha$  concentrates in the pairing-active region near the Fermi energy [19]. It is the spectral gap in even nuclei which is used to calibrate the pairing strength by comparison with the experimental  $\Delta_q^{(3)}$  [32]. A fully consistent computation of odd nuclei allows to check the resemblance of the spectral gap and  $\Delta_q^{(3)}$ .



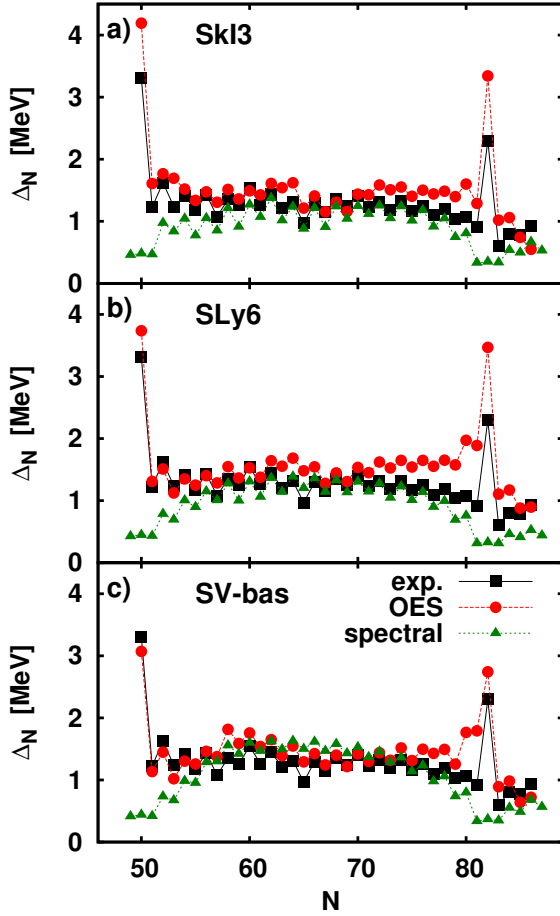


**Fig. 9.** Neutron gaps in Sn isotopes for three different Skyrme forces. Compared are the experimental gap from OES  $\Delta_{N,exp}^{(3)}$ , the theoretical gap from OES  $\Delta_{N,min+s^2}^{(3)}$ , and the spectral gap as defined in eq. (18).

Fig. 9 shows the spectral neutron gap  $\bar{\Delta}_N$  together with the theoretical OES  $\Delta_{N,min+s^2}^{(3)}$  and experimental  $\Delta_N^{(3)}$  in Sn isotopes. There is an acceptable agreement between  $\bar{\Delta}_N$  and  $\Delta_{N,min+s^2}^{(3)}$  in the mid-shell region but a large deviation in trend and magnitude near shell closures where pairing shrinks and shell effects dominate. The magnitude of deviation depends on the parameterization, which confirms its shell origin. The deviations in the mid-shell region stay in a range of about 10% and justify the resemblance of  $\bar{\Delta}_N$  and  $\Delta_{N,min+s^2}^{(3)}$  as a first guess. The theoretical results reproduce nicely the experimental data in the pairing-dominated mid-shell regions, which is not surprising since just these regions were used for the fit of the pairing strength.

Fig. 10 gives the similar comparison for the proton gaps in N=82 isotones. There is again a huge mismatch between  $\bar{\Delta}_Z$  and  $\Delta_{Z,min+s^2}^{(3)}$  near the Z=50 shell closure. However the agreement in the mid shell region is not as good as for the neutron gaps and strongly depends on the Skyrme parameterization. It is thus likely that shell effects

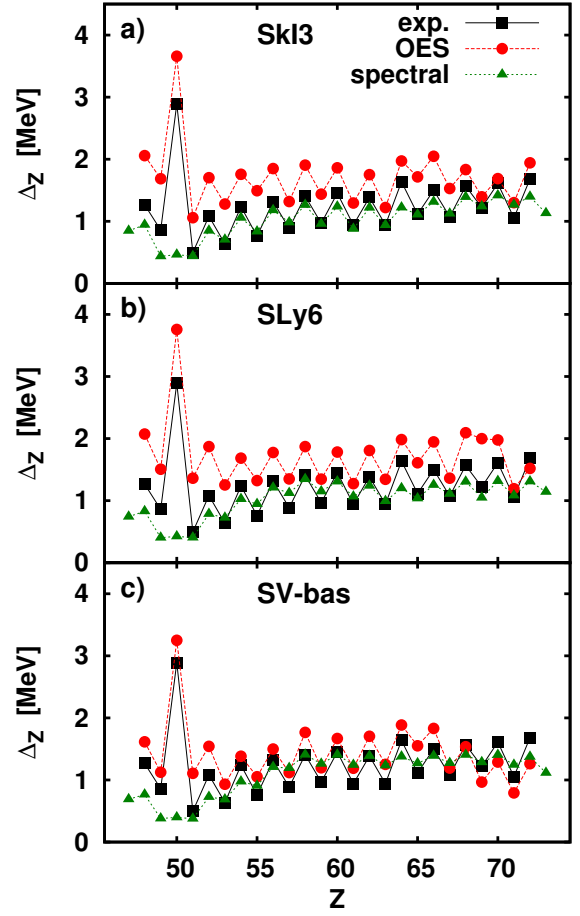


**Fig. 10.** The same as figure 9 for proton gaps in the isotonic chain N=82.

continue to contribute even far off the shell closure. Note that the deviation is smallest for SV-bas.

It is interesting to note that one sees clearly that the spectral gap  $\bar{\Delta}$  was fitted to the experimental OES in even nuclei which shows still good enough agreement even in this case having generally large deviations.

The sensitivity of OES to the pairing strength is tested in figure 11. The result corroborates the finding of the previous two figures. The pairing does not affect the regions near shell closures but dominates mid shell. The changes in the gaps are rather constant in mid shell and exceed those in the pairing strengths (30% versus 20%). A similar amplification was previously found in [50].

### 3.4 Separation energies

The neutron and proton separation energies (SE)

$$S_N(Z, N) = E(Z, N) - E(Z, N - 1), \quad (19)$$

$$S_Z(Z, N) = E(Z, N) - E(Z - 1, N) \quad (20)$$

represent an important nuclear characteristics. They are sensitive to all aspects of the nuclear mean field and pairing. Since SE deal with odd or/and odd-odd nuclei, they can be influenced by TOMF.

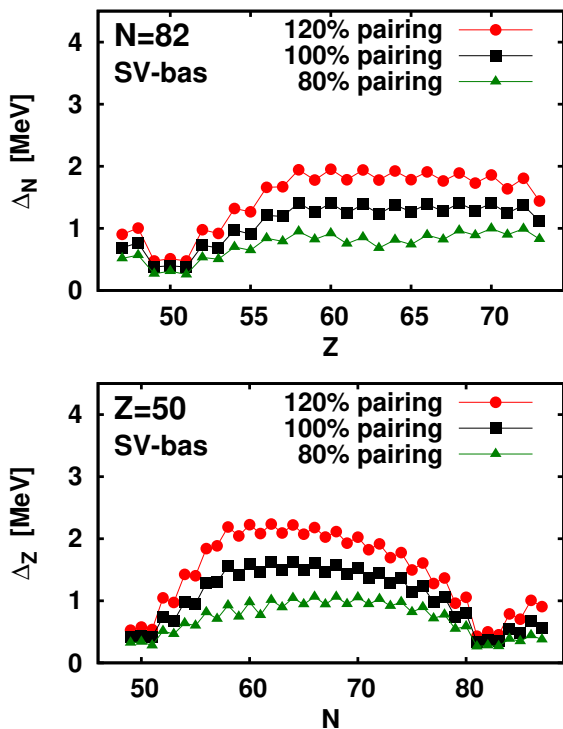


**Fig. 11.** Theoretical OES gaps for varied pairing strength. Upper:  $\Delta_{Z,\min+s^2}^{(3)}$  in the isotones with  $N=82$ . Lower:  $\Delta_{N,\min+s^2}^{(3)}$  in the Sn isotopes.

Figs. 12 and 13 show the systematics of the deviations of SHF neutron and proton SE from the experimental data [46]. There are pronounced errors along isotonic chains for  $S_N$  and isotopic chains for  $S_Z$ . They sensitively depend on the parameterization and are minimal for SV-bas. Obviously this is a shell effect. SE show a large jump at shell closures and size of the jump is closely related to the OES magnitude near the closure. The OES in turn, depends sensitively on the effective mass of the underlying model. The differences near the shell closures in Figs. 12 and 13 are thus related to the effective masses of SHF parameterizations as well. The good performance of SV-bas indicates once more that its effective mass of 0.9 is favorable. The regions of well deformed nuclei (remote from the magic Z and N lines) show generally smaller deviations for all parameterizations. Instead the transitional regions (close to the magic Z and N lines) exhibit larger errors. The latter is probably caused by missing the correlations which are known to be most strong for transitional nuclei.

Table 3 summarizes the r.m.s. deviations for SE. A large difference in performance for the three parameterizations is seen, where SV-bas shows the best results. The difference between various options of the energy functional is smaller. In particular,  $E_{\min+s^2}$  gives a slight improvement of the overall quality. Figs. 12-13 and Table 3 altogether indicate that the choice of the proper Skyrme parameterization is crucial to achieve a good quality of the SE description in all regions of the nuclear chart. Transitional nuclei may require the correlation effects.

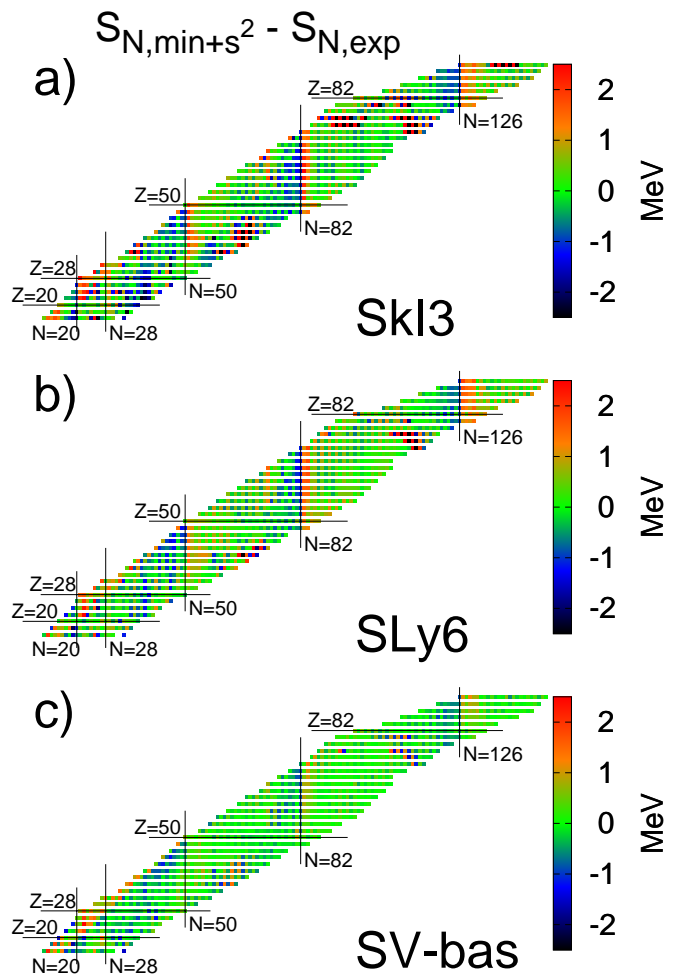


**Fig. 12.** The systematics of difference between SHF and experimental [46] neutron separation energies,  $S_{N,\min+s^2} - S_{N,\exp}$ , drawn in the  $N$ - $Z$ -plane for the parameterizations SkI3, SLy6, and SV-bas.

**Table 3.** R.m.s. deviations (in MeV) between SHF and experimental data [46] for separation energies  $S_{N,Z}$  from Figs. 12-13.

$S_N$	SkI3	SLy6	SV-bas
$E_{\text{even}}$	1.15	0.83	0.50
$E_{\text{min}}$	1.16	0.85	0.50
$E_{\min+s^2}$	0.80	0.60	0.50
$S_Z$	SkI3	SLy6	SV-bas
$E_{\text{even}}$	0.96	0.83	0.53
$E_{\text{min}}$	0.98	0.87	0.54
$E_{\min+s^2}$	0.97	0.82	0.50

### 3.5 Excitation spectra of odd nuclei

The excitation spectrum of odd nuclei is closely related to the single-particle spectrum of the even-even neighbor. In a simple picture one even may deduce the single-particle spectra of the even-even nucleus from the excitations of

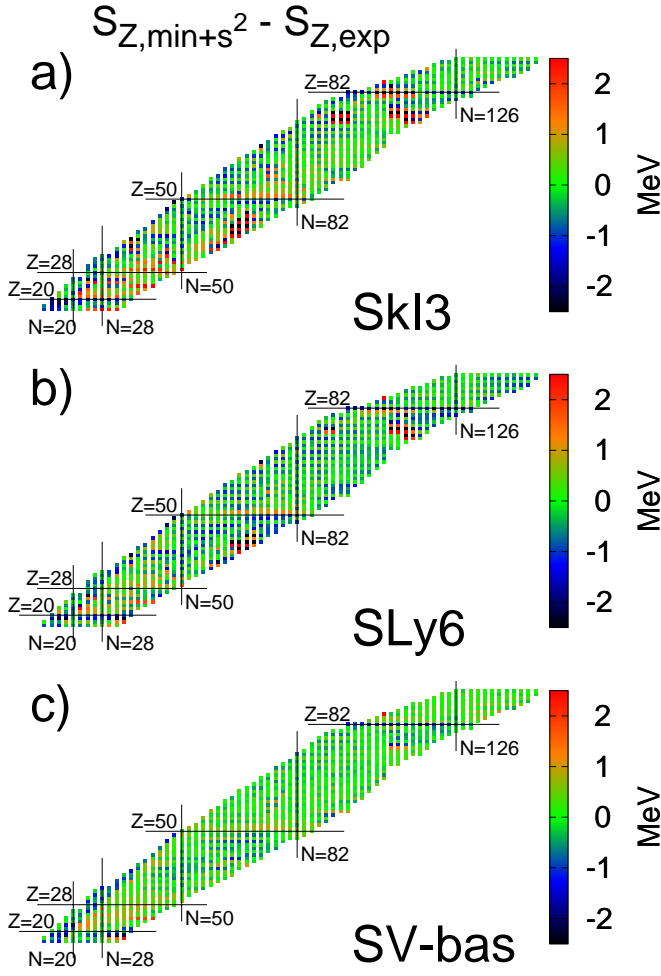


**Fig. 13.** The same as in Fig. 12 for the proton separation energies  $S_Z$ .

the nearby odd systems. We will now check in more detail the effect of TOMF on the excitation energies of odd nuclei and the performance of the simple estimate in terms of the single-particle spectra of the even-even reference system. The comparison with the experimental data will be also done. Here, however, one has to keep in mind that the low-energy excitation spectra of odd nuclei may be heavily influenced by admixture of vibrational states of the even-even core, resulting in a general essential compression of the low energy spectrum. [40,41].

Figure 14 shows the excitation spectra in  $^{207}\text{Pb}$ . This nucleus has a neutron hole with respect to  $^{208}\text{Pb}$ . The simple excitation model is then deduced from the neutron one-hole (1h) and one-particle-two-hole (1p2h) excitation spectra in  $^{208}\text{Pb}$ , as indicated in the figure. In this model, the low-energy spectrum is dominated by 1h excitations but at higher energies the 1p2h excitations become energetically competitive. Such prescription is widely used in various approaches, see e.g. [39,40,41], and it obviously does not include the TOMF effects.

These effects are illustrated in Fig. 14 for the options *even*, *mean*, and *min* +  $s^2$  where the TOMF are added

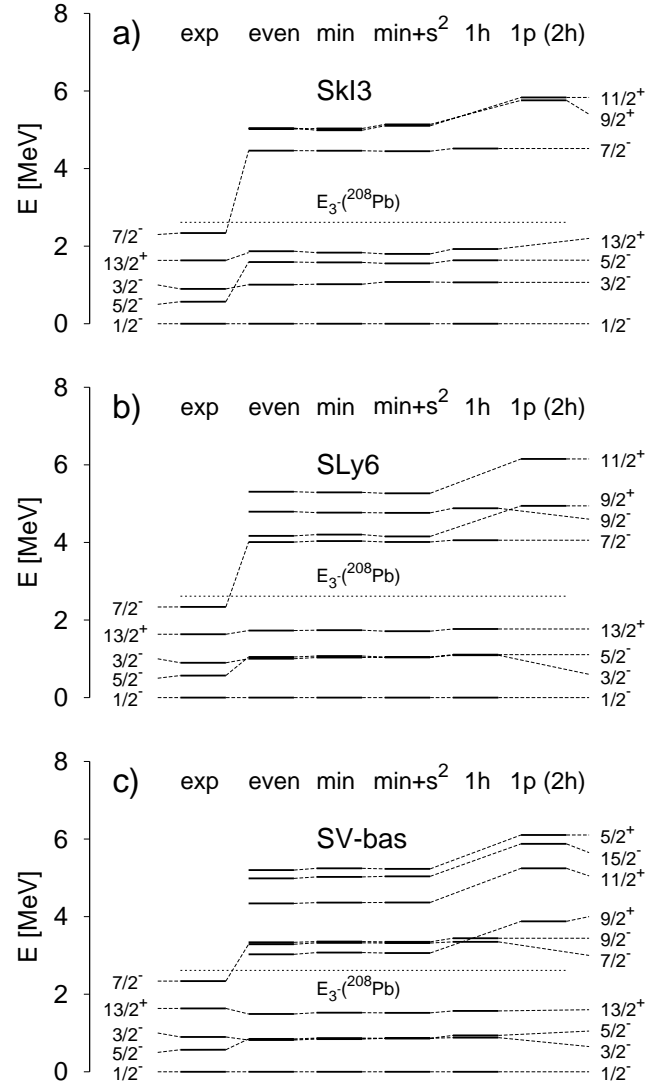


**Fig. 14.** Excitation neutron spectra in  $^{207}\text{Pb}$  for the parameterizations SkI3 (a), SLy6 (b), and SV-bas (c). In every panel, the experimental data [51] are compared with the SHF results for the options (10)-(12). Also the simple one-hole (1h) and one-particle-two-hole (1p2h) estimates from the single-neutron spectrum of  $^{208}\text{Pb}$  are exhibited. The dotted horizontal line marks energy of the lowest collective state  $3^-$  in  $^{208}\text{Pb}$ . For better view, results for one and the same level are connected by dash lines. See text for more details.

step by step. Unlike the simple model discussed above, these results are consistent in the sense that for every state the SHF problem is solved independently by minimization of the total energy. As seen from the figure, the TOMF impact is negligible. At the same time we have strong rearrangement effect for 1p2h states, which is only accounted for the self-consistent mean-field calculations. This makes the simple estimations less reliable, although they still yield a nice first guess.

Comparison with the experimental spectra shows that the calculated levels below 2 MeV follow the right se-

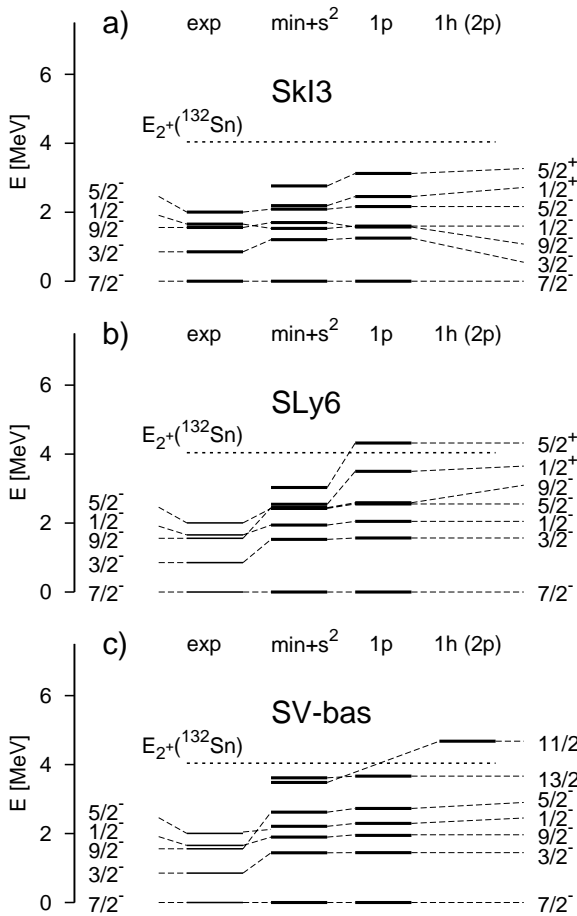


**Fig. 15.** The same as in Fig. 14 but for the neutron spectrum in  $^{133}\text{Sn}$  and the option  $\text{min} + s^2$  alone. The dotted line marks the lowest collective state  $2^+$  in reference even-even core  $^{132}\text{Sn}$ . The experimental data are taken from [52].

quence and rather well reproduce the experimental energies, especially for SLy6 and SV-bas. Discrepancies start for the  $7/2^-$  state which has too high energy in all predictions. Most probably this is caused by omitting the vibrational admixture which generally lower and compress the low-energy spectrum. Figure 14 shows the energy of the lowest collective state  $3^-$  in the even-even core  $^{208}\text{Pb}$ , which can serve as a rough energy indicator of the onset of core vibrational admixture. (A more complete estimate would, of course, require to know also the coupling matrix elements.)

Results of similar calculations for neutron-excess nucleus  $^{133}\text{Sn}$  are shown in Fig. 15. This is the case where the neutron particle (1p) states in  $^{132}\text{Sn}$  are explored. Different TOMF options are again found to make a negligible difference. Thus we display here only results from the final option  $\text{min} + s^2$ . The simple 1p estimate provides a nice first guess whose reliability, however, fades with increasing excitation energy, particularly if one approaches the vicinity of the  $2^+$  core excitation. The comparison with the experimental energies in  $^{133}\text{Sn}$  is less convincing than in  $^{207}\text{Pb}$ . All excitation energies are overestimated. This

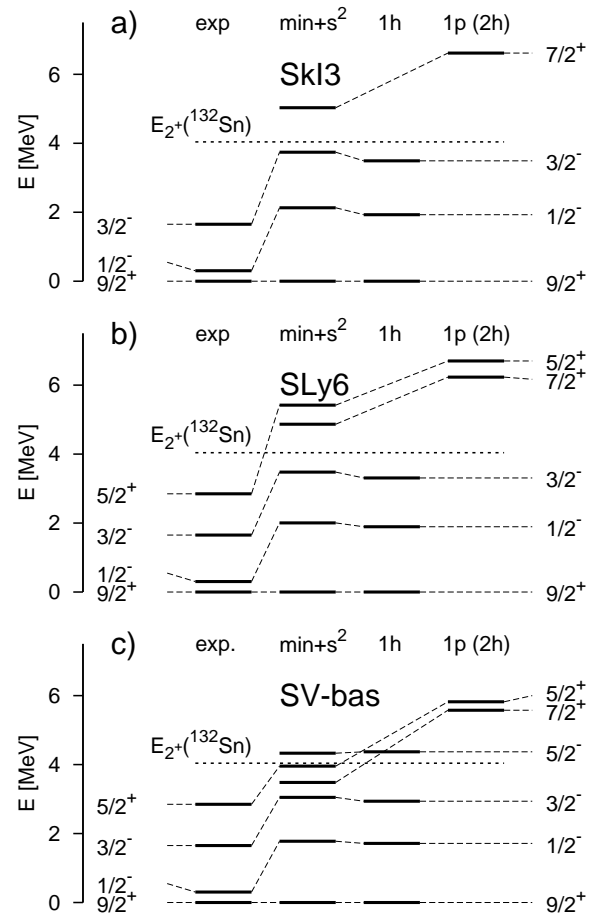


**Fig. 16.** The same as in Fig. 15 for the proton spectrum in  $^{131}\text{In}$ . The reference even-even core is  $^{132}\text{Sn}$ . The experimental data are taken from [53].

is not a problem of spectral density because all three parameterizations yield about the same trends. The most probable reason of the mismatch could be neglecting the core vibrational admixture whose impact in  $^{133}\text{Sn}$  might be stronger than in  $^{207}\text{Pb}$  and so affect even the lowest excitations. The comparison of the simple estimations with the  $\text{min} + s^2$  case exhibits a strong rearrangement effect pertinent to self-consistent calculations.

Fig. 16 shows the spectra for  $^{131}\text{In}$ , the proton-hole neighbor of  $^{132}\text{Sn}$ . The general trends are very similar to the previous figure. Again the simple 1h spectrum provides a good first guess, there is a strong rearrangement effect, and the calculated energies overestimate the experimental data. The later problem appears for all neighbors of  $^{132}\text{Sn}$  while the neighbors of  $^{208}\text{Pb}$  perform fairly well. This systematic deviation is still awaiting an explanation.

## 4 Conclusions

In this paper, we have discussed the description of odd-even and even-odd nuclei in the framework of the Skyrme-Hartree-Fock (SHF) method with BCS pairing. Particular

attention was paid to the influence of the time-odd mean fields (TOMF) in the Skyrme functional which are brought into action by the breaking of time-reversal symmetry through the odd nucleon. Three options were compared: *even* with time-even terms only and omitted TOMF, *min* with adding the minimum of TOMF to restore the Galilean invariance, and *min + s<sup>2</sup>* with additional spin couplings. Gradient spin couplings were omitted as leading to instabilities. The odd nuclei were computed within BCS with blocking the state occupied by the odd nucleon. A bunch of blocked states was computed self-consistently thus yielding the ground state and first few excitations in the odd nucleus. The nuclear properties which might be affected by TOMF, binding energies (BE), odd-even staggering (OES), separation energies (SE) and low-energy single-particle spectra were systematically investigated with three Skyrme parameterizations SkI3, SLy6, and SV-bas for the nuclear chart with  $16 \leq Z \leq 92$ .

The TOMF effects are found generally small and for the spectra even negligible. They affect the results much weaker than the choice of the Skyrme parameterization or rearrangement in self-consistent calculations. For BE, the TOMF effect is maximal for light nuclei and rapidly decreases with increasing nuclear mass number, in accordance to the previous results [18,26]. The change in BE is 100 - 300 keV and TOMF may lead to both less and more binding, depending on the Skyrme parameterizations. The BE description is best with the minimal Galilean invariant option *min* while OES and SE prefer the full functional option *min + s<sup>2</sup>*. The OES can be modified by  $\sim 200$  keV and SE by  $\sim 200$  keV. These results are fluctuations and sometimes conflicting since the currents and spin densities give opposite contributions and partly compensate each other, thus producing a fragile balance. Obviously, so weak and unstable TOMF effects cannot be used for the upgrade of the Skyrme functional in the spin channel.

Some additional important points should be mentioned. First of all, the primary importance of the proper choice of the Skyrme parameterization has to be emphasized. This affects the results much more than TOMF. For all the nuclear characteristics considered in the present exploration, the best description was obtained with the recent parameterization SV-bas. Note that SV-bas has a large effective mass  $m^*/m = 0.9$  and its fit involves isotopic as well as isotonic chains.

Second, differences of binding energies, like OES and SE, are especially sensitive to the shell and pairing details. The OES is dominated by pairing in the mid shell regions and by shell effects near shell closures. Thus a strong dependence on the SHF parameterization is seen at shell closures and very little in mid shell regions where the agreement with experimental OES is generally satisfying. It ought to be reminded that the pairing strength is calibrated to the spectral gap which deviates from OES. Hence the relation between these pairing characteristics was analyzed.

Third, low lying excitation spectra for odd nuclei next to doubly magic ones have been analyzed. There are cases which work nicely and others which do not fit so well. The

mismatch is probably caused by the coupling with vibrational and rotational modes of the even-even core. They are especially strong in deformed and transitional nuclei. The correlations could considerably improve the description of BE, OES, and SE, first of all in mid shell nuclei. Besides, the correlations could be of a crucial importance for description of the low-energy single-particle spectra of odd nuclei. Being too dilute in the mean-field picture, the spectra can become more compressed and closer to the experimental data.

V.O.N. thanks the support from DFG RE-322/12-1 and Heisenberg-Landau (Germany - BLTP JINR) grants.

## A Relation between parameters of the functional

The SHF method can be alternatively formulated by starting since the density-dependent zero-range Skyrme force

$$\hat{V}_{Skyrme} = \hat{V}_{12} + \hat{V}_{dd} + \hat{V}_{LS} \quad (21)$$

$$\hat{V}_{12} = t_0(1 + x_0\hat{P}_\sigma)\delta(\mathbf{r}_1 - \mathbf{r}_2) \quad (22)$$

$$+ \frac{t_1}{2}(1 + x_1\hat{P}_\sigma)\delta(\mathbf{r}_1 - \mathbf{r}_2)\hat{\mathbf{k}}^2$$

$$+ \frac{t_1}{2}(1 + x_1\hat{P}_\sigma)\hat{\mathbf{k}}'^2\delta(\mathbf{r}_1 - \mathbf{r}_2)$$

$$+ t_2(1 + x_2\hat{P}_\sigma)\hat{\mathbf{k}}\delta(\mathbf{r}_1 - \mathbf{r}_2)\hat{\mathbf{k}}$$

$$\hat{V}_{dd} = \frac{t_3}{6}(1 + x_3\hat{P}_\sigma)\rho^\alpha\left(\frac{\mathbf{r}_1 + \mathbf{r}_2}{2}\right)\delta(\mathbf{r}_1 - \mathbf{r}_2) \quad (23)$$

$$\hat{V}_{LS} = it_4(\hat{\boldsymbol{\sigma}}_1 + \hat{\boldsymbol{\sigma}}_2) \cdot \hat{\mathbf{k}}' \times \delta(\mathbf{r}_1 - \mathbf{r}_2)\mathbf{k} \quad (24)$$

with the spin-exchange operator  $\hat{P}_\sigma = \frac{1}{2}(1 + \hat{\boldsymbol{\sigma}}_1\hat{\boldsymbol{\sigma}}_2)$ , the difference momentum  $\hat{\mathbf{k}} = -\frac{i}{2}\left(\vec{\nabla}_1 - \vec{\nabla}_2\right)$  acting to the right, and its counterpart  $\hat{\mathbf{k}}' = \frac{i}{2}\left(\overleftarrow{\nabla}_1 - \overleftarrow{\nabla}_2\right)$  acting to the left. Then the SHF functional (6-9) is obtained as the expectation value of this force with a Slater state. This yields one-to-one correspondence of the force parameters  $t_i, x_i$  with the parameters  $b_i, b'_i, \tilde{b}_i, \tilde{b}'_i$  from (6-9):

$$\begin{aligned} b_0 &= t_0(1 + \frac{1}{2}x_0) & b'_0 &= t_0(\frac{1}{2} + x_0) \\ b_1 &= \frac{t_1}{4}(1 + \frac{1}{2}x_1) & b'_1 &= \frac{t_1}{4}(\frac{1}{2} + x_1) \\ &+ \frac{t_2}{4}(1 + \frac{1}{2}x_2) & &- \frac{t_2}{4}(\frac{1}{2} + x_2) \\ b_2 &= \frac{3t_1}{8}(1 + \frac{1}{2}x_1) & b'_2 &= \frac{3t_1}{8}(\frac{1}{2} + x_1) \\ &- \frac{t_2}{8}(1 + \frac{1}{2}x_2) & &+ \frac{t_2}{8}(\frac{1}{2} + x_2) \\ b_3 &= \frac{1}{4}t_3(1 + \frac{1}{2}x_3) & b'_3 &= \frac{1}{4}t_3(\frac{1}{2} + x_3) \\ b_4 &= \frac{1}{2}t_4 & b'_4 &= \frac{1}{2}t_4 \\ \tilde{b}_0 &= \frac{1}{4}t_2x_0 & \tilde{b}'_0 &= \frac{1}{4}t_0 \\ \tilde{b}_1 &= \frac{1}{8}(t_1x_1 + t_2x_2) & \tilde{b}'_1 &= \frac{1}{8}(t_1 - t_2) \\ \tilde{b}_2 &= \frac{1}{16}(3t_1x_1 - t_2x_2) & \tilde{b}'_2 &= \frac{1}{16}(3t_1 + t_2) \\ \tilde{b}_3 &= \frac{1}{24}t_3x_3 & \tilde{b}'_3 &= \frac{1}{24}t_3 \end{aligned} \quad (25)$$

## B Single-particle wave function

The single-particle wave function in the cylindrical coordinates is the spinor

$$\phi_k(\mathbf{r}) = \begin{pmatrix} \phi_k^{(+)}(\mathbf{r}) \\ \phi_k^{(-)}(\mathbf{r}) \end{pmatrix} = \begin{pmatrix} R_k^{(+)}(\rho, z)e^{im_k^{(+)}\vartheta} \\ R_k^{(-)}(\rho, z)e^{im_k^{(-)}\vartheta} \end{pmatrix}, \quad (26)$$

with

$$m_k^{(s)} = K_k - \frac{1}{2}s, \quad m_k^{(-s)} = K_k + \frac{1}{2}s \quad (27)$$

and  $K_k$  is the projection of the total momentum of k-state on the symmetry z-axis.

## References

1. M. Bender, P.-H. Heenen, and P.-G. Reinhard, *Rev. Mod. Phys.* **75**, 121 (2003).
2. D. Vretenar, A.V. Afanasjev, G.A. Lalazissis, and P. Ring, *Phys. Rep.* **409**, 101 (2005).
3. J. R. Stone and P.-G. Reinhard, *Prog. Part. Nucl. Phys.* **58**, 587 (2007).
4. Y.M. Engel, D.M. Brink, K. Goeke, S.J. Krieger, and D. Vauterin, *Nucl. Phys. A* **249**, 215 (1975).
5. J. Dobaczewski and J. Dudek, *Phys. Rev. C* **52**, 1827 (1995).
6. A.V. Afanasjev and P. Ring, *Phys. Rev. C* **62**, 031302(R) (2000).
7. H. Zduńczuk, W. Satula, and R.A. Wyss, *Phys. Rev. C* **71**, 024305 (2005).
8. A.V. Afanasjev, *Phys. Rev. C* **78**, 054303 (2008).
9. V.O. Nesterenko, J. Kvasil, and P.-G. Reinhard, *Phys. Rev. C* **66**, 044307 (2002).
10. V.O. Nesterenko, W. Kleinig, J. Kvasil, P.-G. Reinhard, and P. Vesely, *Phys. Rev. C* **74**, 054306 (2006).
11. W. Kleinig, V.O. Nesterenko, J. Kvasil, P.-G. Reinhard and P. Vesely, *Phys. Rev. C* **78**, 044313 (2008).
12. V.O. Nesterenko, W. Kleinig, J. Kvasil, P. Vesely, and P.-G. Reinhard, *Int. J. Mod. Phys. E* **17**, 89, (2008).
13. P. Vesely, J. Kvasil, V.O. Nesterenko, W. Kleinig, P.-G. Reinhard, and V.Yu. Ponomarev, *Phys. Rev. C* **80**, 031302(R)(2009).
14. V.O. Nesterenko, J. Kvasil, P. Vesely, W. Kleinig, P.-G. Reinhard, and V.Yu. Ponomarev, *J. Phys. G: Nucl. Part. Phys.* **37**, 064034 (2010).
15. K. Langanke and M. Wiescher, *Rep. Prog. Phys.* **64**, 1657 (2001).
16. J. Dobaczewski, H. Flokard, and J. Treiner, *Nucl. Phys. A* **422**, 103 (184).
17. K. Rutz, M. Bender, P.-G. Reinhard, J.A. Maruhn and W. Greiner, *Nucl. Phys. A* **634**, 67 (1998).
18. W. Satula, in *Nuclear Structure 98*, edited by C. Baktash, AIP, Conf. Proc. **481** (AIP, New York, 1999), p. 114; arXiv:nucl-th/9809089.
19. M. Bender, K. Rutz, P.-G. Reinhard, and J.A. Maruhn, *Eur. Phys. J. A* **8**, 59 (2000).
20. T. Duguet, P. Bonche, P.-H. Heenen, and J. Meyer, *Phys. Rev. C* **65**, 014310 (2001); *ibid.*, **65**, 014311 (2001).
21. C.A. Bertulani, H.F. Liu, and H. Sagawa, *Phys. Rev. C* **80**, 027303 (2009).
22. G.F. Bertsch, C.A. Bertulani, W. Nazarewicz, N. Schunck, and M.V. Stoitsov, *Phys. Rev. C* **79**, 034306 (2009).
23. Yu. E. Penionzhkevich and S.M. Lukyanov, *Phys. Part. Nucl.*, **37**, 1 (2006).
24. Z. Ren, D.-H. Chen, F. Tai, H.Y. Zhang, and W.Q. Shen, *Phys. Rev. C* **67**, 064302 (2003).
25. L. Ahmad, J.P. Greene, E.F. Moore, F.G. Kondev and R.R. Chasman, *Phys. Rev. C* **72**, 058308 (2005); J. Qian et al, *Phys. Rev. C* **79**, 064319 (2009).
26. A.V. Afanasjev and H. Abusara, *Phys. Rev. C* **81**, 014309 (2010).
27. K.-Y. Passler, *Nucl. Phys. A* **257**, 253 (1976).
28. M. Beiner, H. Flocard, Nguen Van Giai, And P. Quentin, *Nucl. Phys. A* **238**, 29 (1975).
29. E. Chabanat, P. Bonche, P. Haensel, J. Meyer, and R. Schaeffer, *Nucl. Phys. A* **627**, 710 (1997).
30. N. Schunck, J. Dobaczewski, J. McDonnell, J. Moré, W. Nazarewicz, J. Sarich, and M. V. Stoitsov1, *Phys. Rev. C* **81**, 024316 (2010).
31. P.-G. Reinhard and H. Flocard, *Nucl. Phys. A* **584**, 467 (1995).
32. P. Klüpfel, P.-G. Reinhard, T.J. Bürvenich and J.A. Maruhn *Phys. Rev. C* **79** 034310 (2009)
33. T.H.R. Skyrme, *Phil. Mag.* **1**, 1043 (1956).
34. D. Vauterin, D.M. Brink, *Phys. Rev. C* **5**, 626 (1972).
35. T. Lesinski, K. Bennaceur, T. Duguet, and J. Meyer, *Phys. Rev. C* **74**, 044315 (2006).
36. M. Kortelainen and T. Lesinski, *J. Phys. G* **37**, 064039 (2010).
37. J. Erler, P. Klüpfel, and P.-G. Reinhard, *Eur. Phys. J A* **37**, 81 (2008).
38. S.J. Krieger, P. Bonche, H. Flocard, P. Quentin, and M.S. Weiss, *Nucl. Phys. A* **517**, 275 (1990).
39. P. Ring and P. Schuck, *The nuclear many-body problem* (Springer-Verlag, Berlin, 1980).
40. V.G. Soloviev, *Theory of complex nuclei*, (Pergamon Press, Oxford, 1976).
41. F.A. Gareev, S.P. Ivanova, L.A. Malov, and V.G. Soloviev, *Nucl. Phys. A* **171**, 134 (1971).
42. B.A. Alikov, Kh.N. Badalov, V.O. Nesterenko, A.V. Sushkov, and J. Wawryszczuk, *Z. Phys. A* **331** 265 (1988).
43. V.O. Nesterenko, *Sov. J. Part. Nucl.* **24** 1517 (1993).
44. P. Klüpfel, J. Erler, P.-G. Reinhard, and J.A. Maruhn, *Eur. Phys. J. A* **37**, 343 (2008).
45. S. Goriely, F. Tondeur, and J. M. Pearson, *At. Data Nucl. Data Tables* **f 77**, 311 (2001).
46. G. Audi, A.H. Wapstra, and C. Thibault, *Nucl. Phys. A* **729** 337 (2003).
47. J. Erler, P. Klüpfel, and P.-G. Reinhard, *J. Phys. G* **37**, 064001 (2010).
48. J. Dobaczewski, W. Nazarewicz, T.R. Werner, J.F. Berger, C.R. Chinn, and J. Dechargé, *Phys.Rev. C* **53**, 2809 (1996).
49. J. Dobaczewski, P. Magierski, W. Nazarewicz, W. Satula, and Z. Szymanski, *Phys. Rev. C* **63** 024308 (2001).
50. K. Rutz, M. Bender, P.-G. Reinhard, and J.A. Maruhn, *Phys. Lett. B* **468**, 1 (1999).
51. M.R. Schmorak, *Nucl. Data Sheets* **43**, 383 (1984); M. J. Martin, *Nucl. Data Sheets* **70**, 315 (1993).
52. Yu.V. Sergeenkov and V.M. Sigalov, *Nucl. Data Sheets* **49**, 639 (1986); Sh. Rab, *Nucl. Data Sheets* **75**, 491 (1995), P. Hoff et al., *Phys. Rev. Lett.* **77**, 1020 (1996).

53. Yu.V. Sergeenkov, Yu.L. Khazov, T.W. Burrows, and M.R. Bhat, Nucl. Data Sheets **72**, 487 (1994); Yu. Khazov, I. Mitropolsky and A. Rodionov, Nucl. Data Sheets **107**, 2715 (2006).